Research Article

Mechanical Characteristics of Fully Grouted and Antiseismic Bolts considering Transverse Deformation in Underground Caverns

Buyun Yang [1,2] **Ming Xiao** [1,2] **Guoqing Liu** [3] **and Juntao Chen** [1,2]

[1]*State Key Laboratory of Water Resources and Hydropower Engineering Science, Wuhan University, Wuhan 430072, China*
[2]*Key Laboratory of Rock Mechanics in Hydraulic Structural Engineering of Ministry of Education, Wuhan University,*
 Wuhan 430072, China
[3]*China Institute of Water Resources and Hydropower Research, Beijing 100048, China*

Correspondence should be addressed to Ming Xiao; mxiao@whu.edu.cn

The load transfer control equations under bolt-surrounding rock interaction are established on the basis of classical beam theory and the trilinear shear slip model. The axial stress and transverse shear force distributions of the anchorage body are obtained by solving the equations. The equivalent forces obtained by the transverse force and axial shear stress of the bolts are applied to rock mass elements to simulate the support effect. A new dynamic algorithm for bolts is proposed in considering of the axial and transverse deformation of the anchorage body. The rationality of the algorithm is verified by comparing with laboratory pullout and shear tests of bolts. A dynamic time-history case study of underground caverns is conducted using this algorithm. Results indicate that (1) the algorithm may reflect the stress and deformation characteristics of bolts during an earthquake; (2) for the antiseismic support effect of the surrounding rock at fault, the bolt algorithm in this study is more valid than the algorithm that considered only the axial deformation of bolts; (3) in the support force of the bolt to the surrounding rock, transverse force is the key to limit fault dislocation and reduce the dynamic damage of the rock at fault.

1. Introduction

Southwest China is rich in water resources and has several hydropower stations. Restricted by geological conditions, these hydropower stations are mainly built across underground rock. The region is located at plate boundaries with a high probability of earthquakes; therefore, the antiseismic performance of underground caverns is directly related to the operational safety of hydropower stations [1]. As a flexible seismic reinforcement measure, bolt support is widely used in mining, water conservancy, and transportation industries due to its economic, simple, and reliable advantages. A commonly used bolt type in underground engineering is fully grouted rock bolt. Rock mass is strengthened by the rigidity and strength of the bolts, and the deformation of the surrounding rock is

limited by transferring shear stress at the interface between the anchorage body and the surrounding rock [2]. Freeman [3] first proposed neutral point theory, which effectively describes the axial stress of a bolt in rock mass and has become important for analyzing bolt-surrounding rock interaction. Recent research on axial mechanical transform mechanisms between the anchorage body and rock mass is mainly based on pullout tests [4–6] and theoretical models [7–9].

The abovementioned studies only considered the effect of axial stress on bolts. However, in an actual rock mass, numerous faults and joint surfaces exist. The bolts not only reinforce the rock mass in the axial direction but also effectively stop or delay the displacement of the joint surface in the transverse direction [10]. Therefore, bolt mechanisms that consider transverse deformation require further

study. The effects of material, dimension, inclination, prestress, bolt profile, rock strength, and joint roughness on the shear resistance of bolts have been studied through tests [11–16]. Pellet and Egger [17] determined the relationships between axial force and deformation and transverse shear force and bolt deformation. Jalalifar and Aziz [18] studied the force and deformation distribution of a shear-stressed bolt in the elastic and plastic stages and showed the relationship between the plastic hinge point and transverse deformation of the bolt. Ge and Liu [19] proposed a theoretical formula for estimating the shear strength of bolted rock joints. Zhang and Liu [20] comprehensively considered the axial and transverse deformability of bolts and proposed a deformation model of bolts under transverse shear load.

Several studies have presented static and dynamic calculations for bolt data using numerical methods in underground caverns [2, 21–23]. However, these studies have considered only the axial effect and neglected the transverse effect of bolts on the surrounding rock. Research on transverse deformation and force of bolts is mainly based on small-scale bolt shear tests and analytical methods. The mechanical characteristics of bolts considering axial and transverse deformation and their support effect on the surrounding rock should be studied further. Therefore, the current study takes underground caverns as research background, considers the axial and transverse deformation of bolts, and establishes the governing equations of load transfer between bolts and the surrounding rock. A new analytical algorithm for a fully grouted bolt, which is suitable for seismic time-history analysis under complex conditions, such as joints and fault, is proposed. The rationality of the algorithm is verified, and a 3D finite element method (FEM) model of underground caverns of a hydropower station is used to study the force and deformation regularity and support effect of bolts under seismic load.

2. Analytical Model for Bolt-Rock Interaction

In this study, the implicit bolt element, which is buried in rock mass element and has no effect on the division of rock mass is used for bolt simulation [24]. This study is mainly based on the following assumptions: (1) the bolt is made of a homogeneous elastic material; (2) the perfect combination between the bolt and mortar causes them to deform together; (3) the slip failure of the bolt only occurs at the interface between mortar and rock; (4) the transverse deformation of anchorage body is consistent with that of the rock.

2.1. Transverse Deformation and Force of Bolt. The mutual displacement between the joint surface of the rock causes the axial displacement u_o and transverse displacement v_o of the bolt, resulting in a similar "S" deformation of the bolt. The mechanical model is shown in Figure 1 [25]. Point O is
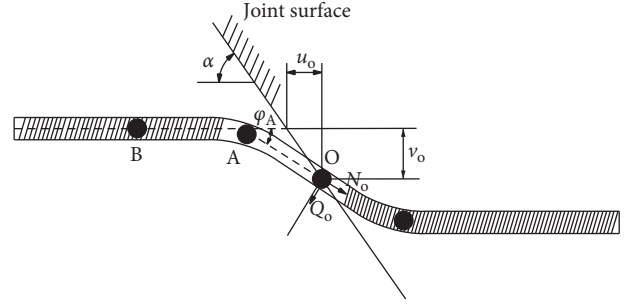

Figure 1: Bolt deformation.

the intersection of the bolt and the joint surface. The rotation angle at point B is 0. The shear force and rotation angle are 0, and the bending moment is the largest at point A [18]. AO is called plastic hinge segment, and A is the plastic hinge point [17]. N_o and Q_o are, respectively, the axial force and transverse shear force generated at point O when the bolt is transversely deformed.

Segment AO in Figure 1 is simplified to a static beam, and the force analysis of this segment is conducted on the basis of classical beam theory, as shown in Figure 2. q_x is the reaction force concentration of the rock on the compression side of the bolt, and its distribution along the bolt is parabolic [10], i.e.,

$$q_x = \frac{q_o}{l^2} x^2, \tag{1}$$

where l is the length of AO, and the expression of l is semiempirical, $l = \sqrt{\sigma_{el} \pi D^3/(\sigma_c v_o)}$ [18]; σ_{el} is the yield strength of the bolt; and σ_c is the compressive strength of the surrounding rock. D is the diameter of anchorage body, $D = D_b + 2t$, where D_b is the diameter of bolt, and t is the thickness of mortar.

The shear force at point A is 0; thus, the force balance analysis of AO is performed as

$$\sum F_y = 0 \Longrightarrow Q_o = \frac{q_o l}{3}. \tag{2}$$

The bending moment $M(x)$ of AO is

$$M(x) = Q_o(l - x) - \frac{q_o x^4}{12l^2} + \frac{1}{3}q_o lx - \frac{1}{4}q_o l^2. \tag{3}$$

On the basis of the differential equation of beam deflection curve, the approximate deflection curve expression of AO can be obtained by the integral of equation (3) as

$$v(x) = \int\int \left[Q_o(l - x) - \frac{1}{4}q_o l^2 + \frac{1}{3}q_o lx - \frac{q_o x^4}{12l^2} \right] + C. \tag{4}$$

The rotation angle and deflection at point A are 0; hence, equation (4) can be transformed as

$$v(x) = \frac{Q_o(l-x)^3}{6EI} - \frac{q_o x^6}{360EIl^2} + \frac{q_o lx^3}{18EI} - \frac{q_o l^2 x^2}{8EI} + \frac{Q_o l^2 x}{2EI} - \frac{Q_o l^3}{6EI}. \tag{5}$$
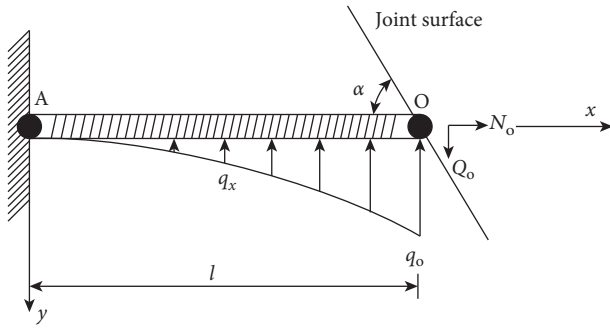
FIGURE 2: Force of segment AO in the bolt.

FIGURE 3: Trilinear shear slip model.

Transverse displacement v_o at point O of the bolt can be obtained by substituting $x = l$ into equation (5) as

$$v_o = \frac{Q_o l^3}{3EI} - \frac{13 q_o l^4}{180 EI}. \tag{6}$$

The transverse load-displacement-controlled equation between the bolt and rock can be obtained by combining equations (2) and (6) into

$$Q_o = \frac{60 v_o EI}{7 l^3}, \tag{7}$$

where E is the equivalent elastic modulus of the anchorage body; E_b and E_m are the elastic moduli of the bolt and mortar, respectively; $E = (E_b A_b + E_m A_m)/A_a$, where A_a, A_b, and A_m are the cross-sectional area of the anchorage body, bolt, and mortar, respectively; I is the moment of inertia of the anchorage body, $I = \pi D^4/64$.

2.2. Axial Deformation and Stress of Bolt

2.2.1. Bond Slip Model for Interface.
The trilinear shear slip model [26] shown in Figure 3 is adopted to describe the relationship between shear stress and shear displacement at the interface. Shear displacement u is the relative displacement between the anchorage body and surrounding rock, i.e.,

$$u = u_r(x) - u_a(x), \tag{8}$$

where $u_r(x)$ and $u_a(x)$ are the respective axial displacements of the surrounding rock and anchorage body at x.

(1) Elastic Stage 1. The anchoring interface is in a linear-elastic state, and the expression is

$$\tau = K_1 u, \tag{9}$$

where K_1 is the shear stiffness of the interface during the elastic stage, which is calculated by the following equation [27]:
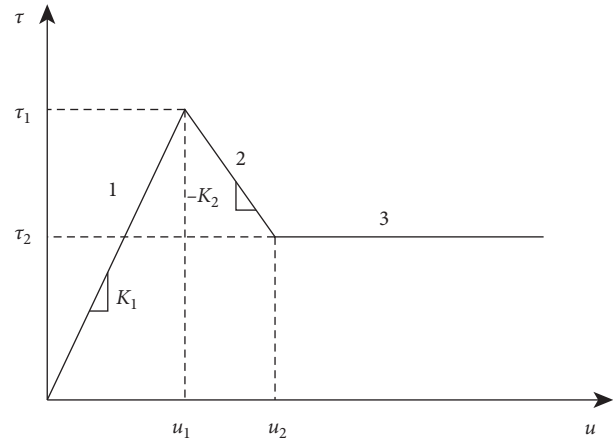
$$K_1 = \frac{K_r K_m}{(K_r + K_m)}, \tag{10}$$

where K_r is the shear stiffness of the rock, which can be valued in accordance with different rock masses; K_r is 5–10 and 1.5–3 GPa/m for hard and soft rock, respectively [1]. K_m is the shear stiffness of mortar, which is calculated by the following equation [28]:

$$K_m = \frac{2 G_m}{[D \ln(1 + 2t/D)]}, \tag{11}$$

where G_m is the shear modulus of mortar; generally, $G_m = 0.4 E_m$.

(2) Plastic Softening Stage 2. Shear stress decreases when the relative displacement increases, and the expression is

$$\tau = \tau_1 - K_2 (u - u_1), \tag{12}$$

where K_2 is the shear stiffness of the interface during the plastic softening stage; τ_1 is the peak shear stress; u_1 is the relative displacement corresponding to τ_1. $\tau_1 = c_i + \sigma_r \tan \varphi_i$, where c_i and φ_i are the cohesive force and internal frictional angle of the interface, respectively; and σ_r is the hydrostatic confining pressure of the rock element perpendicular to the anchoring surface [22].

(3) Residual Strength Stage 3. The interface is completely damaged, and only residual shear stress τ_2 exists, namely,

$$\tau = \tau_2 = \sigma_r \tan \varphi_i. \tag{13}$$

2.2.2. Load Transfer Differential Equation.
A microsegment of the anchorage body, which has a coordinate of x and length of dx, is considered for study. A 1D local coordinate system is established along the axial direction of the anchorage body and has a positive direction from the anchor head to the deep rock. The force and deformation of this anchorage body and rock are shown in Figure 4.

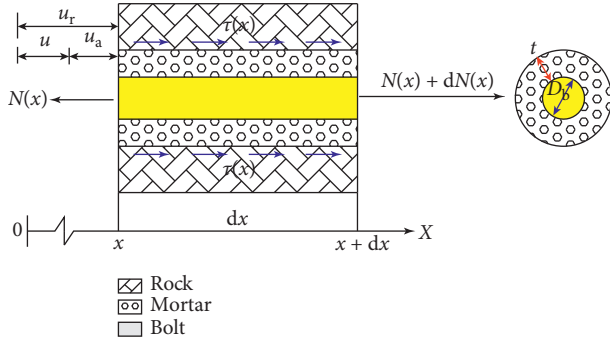The balanced differential equation of the microsegment is

FIGURE 4: Interaction between anchorage body and rock.

$$N(x) + dN(x) - N(x) + \tau(x)\pi D\, dx = 0. \tag{14}$$

The following equation can be derived using equation (14):

$$\frac{d^2 N(x)}{dx^2} + \pi D \frac{d\tau(x)}{dx} = 0. \tag{15}$$

Equations (9) and (12) are derived and, respectively, combined with equation (8), i.e.,

$$\frac{d\tau(x)}{dx} = K_1 [\varepsilon_r(x) - \varepsilon_a(x)], \tag{16}$$

$$\frac{d\tau(x)}{dx} = -K_2 [\varepsilon_r(x) - \varepsilon_a(x)], \tag{17}$$

where $N(x)$ is the axial force of the anchorage body at x; $\tau(x)$ is the shear stress of the anchoring interface; $\varepsilon_r(x)$ and $\varepsilon_a(x)$ are the strains corresponding to $u_r(x)$ and $u_a(x)$, respectively.

In the transverse deformation of the bolt (shown in Figure 1), the axial displacement u_o of the bolt in point O is composed of the deformation caused by N_o and M_A, which can be derived from Hooke's law and the formula of maximum bending moment normal stress [10], i.e.,

$$u_o = \frac{N_o l}{EA_a} + \frac{M_A l}{EW} = \frac{N_o l}{EA_a} + \frac{Q_o l^2}{4EW}. \tag{18}$$

The microsegment shown in Figure 4 is supposed to be a section of a transverse deformation bolt, and x corresponds to point O in Figure 1. The following equation can be deduced from equation (18) via the geometric method:

$$\varepsilon_a(x) = \frac{l}{EA_a} \frac{dN(x)}{dx} + \frac{l^2}{4EW} \frac{dQ(x)}{dx}, \tag{19}$$

where W is the bending section modulus of the anchorage body; $W = \pi D^3/32$; $Q(x)$ is the transverse force of the bolt at x; $Q(x) = 60 v(x)EI/(7l^3)$; $v(x)$ is the transverse displacement of the bolt at x.

The axial controlled equation for the interaction between the rock and anchorage body can be obtained by combining equations (16) and (17) with equations (15) and (19). The unified expression is

$$\frac{d^2 N(x)}{dx^2} - \alpha \frac{dN(x)}{dx} + \beta \frac{du_r(x)}{dx} - \gamma \frac{dQ(x)}{dx} = 0, \tag{20}$$

where $\alpha = \pi DKl/(EA_a)$; $\beta = \pi DK$; and $\gamma = 8Kl^2/(ED^2)$. K is replaced with K_1 in the elastic stage and with $-K_2$ in the plastic softening stage.

3. Solution of the Controlled Equation

After the excavation of underground caverns, the displacement of the surrounding rock is a series of element node displacements in the directions of x, y, and z; the calculated $u_r(x)$ and $Q(x)$ are discrete values. The functional expression of $N(x)$ is difficult to obtain through the analytic method. Thus, the finite difference method is adopted to solve equation (20), thereby obtaining the numerical solution of $N(x)$.

Bolt length is denoted as L and equally divided into n segments along the axial direction. Each segment length is $h = L/n$. The starting point of the bolt near the free surface is $x = 0$, and the end point is $x = L$. The segmented points are numbered in order as 1, 2, ..., $n + 1$. In accordance with the finite difference principle, the corresponding derivatives are replaced with the difference quotient of segmented points, and equation (20) is transformed as

$$\frac{N_{i+1} - 2N_i + N_{i-1}}{h^2} - \alpha \frac{N_{i+1} - N_{i-1}}{2h} + \beta \frac{u_r^{i+1} - u_r^{i-1}}{2h} - \gamma \frac{Q_{i+1} - Q_{i-1}}{2h} = 0, \tag{21}$$

where N_i, u_r^i, and Q_i are the values of $N(x)$, $u_r(x)$, and $Q(x)$ at the i-th segmented point, respectively. The range of i in equation (21) is $2 \le i \le n$. When $i = 1$ and $i = n + 1$, the following boundary conditions are needed:

$$N_1 = N_0; \qquad N_{n+1} = 0, \tag{22}$$

where N_0 is the prestress applied to the anchor head; if no prestress exists, $N_0 = 0$.

$\Delta u_r^i = (u_r^{i+1} - u_r^{i-1})/2$ and $\Delta Q_i = (Q_{i+1} - Q_{i-1})/2$ are taken, and equation (21) can be rewritten in a matrix form as

$$[M][N] + [B][\Delta u_r] + [G] = [C][\Delta Q], \tag{23}$$

where

$$[M] = \begin{bmatrix} -2 & \chi_2 & & & \\ \omega_3 & -2 & \chi_3 & & \\ \ddots & \ddots & \ddots & & \\ & & \omega_{n-1} & -2 & \chi_{n-1} \\ & & & \omega_n & -2 \end{bmatrix},$$

$$[N] = \begin{bmatrix} N_2 \\ N_3 \\ \vdots \\ N_n \end{bmatrix},$$

$$[G] = \begin{bmatrix} N_0 \\ 0 \\ \vdots \\ 0 \end{bmatrix},$$

$$[B] = \begin{bmatrix} h\beta & & & \\ & h\beta & & \\ & & \ddots & \\ & & & h\beta \\ & & & & h\beta \end{bmatrix}, \tag{24}$$

$$[\Delta u_r] = \begin{bmatrix} \Delta u_r^2 \\ \Delta u_r^3 \\ \vdots \\ \Delta u_r^n \end{bmatrix},$$

$$[C] = \begin{bmatrix} h\gamma_2 & & & \\ & h\gamma_3 & & \\ & & \ddots & \\ & & & h\gamma_{n-1} \\ & & & & h\gamma_n \end{bmatrix},$$

$$[\Delta Q] = \begin{bmatrix} \Delta Q_2 \\ \Delta Q_3 \\ \vdots \\ \Delta Q_n \end{bmatrix}.$$

Equation (23) is a tridiagonal linear equation system for $n-1$ element unknown variable $[N]$, which can be solved using the Chase method. When the interface is in different stages, the values of parameters in equation (23) are different.

(1) Elastic stage 1:

$$\begin{cases} \chi_i = 1 - \dfrac{\alpha h}{2}, \omega_i = 1 + \dfrac{\alpha h}{2}, \alpha = \dfrac{\pi D K_1 l_i}{E A_a}, \\[3mm] \beta = \pi D K_1, \gamma = \dfrac{8 K_1 l_i^2}{E D^2}. \end{cases} \tag{25}$$

(2) Plastic softening stage 2:

$$\begin{cases} \chi_i = 1 - \dfrac{\alpha' h}{2}, \omega_i = 1 + \dfrac{\alpha' h}{2}, \alpha' = \dfrac{-\pi D K_2 l_i}{E A_a}, \\[3mm] \beta' = -\pi D K_2, \gamma' = \dfrac{-8 K_2 l_i^2}{E D^2}. \end{cases} \tag{26}$$

(3) Residual strength stage 3:

$$\tau_i = \tau_2, \tag{27}$$

where $l_i = \sqrt{\sigma_{el} \pi D^3 / (\sigma_c v_i)}$ and v_i is the transverse displacement at the i-th segmented point of the bolt.

The expression of $\tau(x)$ can be obtained by transforming equation (14) into

$$\tau(x) = -\frac{1}{\pi D} \frac{dN(x)}{dx}. \tag{28}$$

$N_0 = N_1$ and $N_{n+2} = N_{n+1}$ are taken, and equation (28) is discretized by the finite difference method. The values of $\tau(x)$ and $\sigma(x)$ at different segmented points can be calculated by

$$\tau_i = \begin{cases} -\dfrac{1}{\pi D} \dfrac{N_2 - N_1}{h}, & i = 1, \\[3mm] -\dfrac{1}{2\pi D} \dfrac{N_{i+1} - N_{i-1}}{h}, & 2 \le i \le n, \\[3mm] -\dfrac{1}{\pi D} \dfrac{N_{n+1} - N_n}{h}, & i = n+1, \end{cases} \tag{29}$$

$$\sigma_i = \frac{4 N_i}{\pi D^2}. \tag{30}$$

4. Dynamic Calculation Theory with Bolt Support

With regard to the dynamic finite element calculation of underground caverns, the differential equation of motion by the Lagrange method is established as [29].

$$M\ddot{a} = f_{ext} - f_{int} - C\dot{a}, \tag{31}$$

where M and C are the lumped mass and damping matrices of the model nodes, respectively; $\ddot{a}$ and $\dot{a}$ are the acceleration and velocity of the nodes, respectively; f_{ext} and f_{int} are the external and internal forces of the nodes, respectively.

4.1. Mechanism of Bolt Support. The mechanical restraint of the bolt to the surrounding rock is reflected by its support reaction force f_{mg}. The dynamic calculation differential equation under bolt support is obtained by substituting f_{mg} into equation (31) as

$$M\ddot{a} = f_{ext} - f_{int} - C\dot{a} + f_{mg}. \tag{32}$$

The axial shear stresses at the interface can be equivalently transformed into concentrated loads at the segmented points. The loads are exerted on the rock elements in an opposite direction, which can simulate the axial support effect of bolts. The shear stresses are supposed to be linearly distributed on the anchoring interface, and the equivalent load of each segmented point is expressed as

$$T_i = \frac{\pi Dh(\tau_i + \tau_{i+1})}{2}, \quad 1 \le i \le n, \tag{33}$$

The three components of T_i in the global coordinate system of the model are given as

$$\{T_i^x \ T_i^y \ T_i^z\}^{\mathrm{T}} = \{p \ s \ w\}^{\mathrm{T}} T_i, \tag{34}$$

where p, s, and w are the directional cosines of the bolt.

The plastic hinge segment l_i at each segmented point must be calculated in accordance with the σ_c of the rock element where the segmented point is located. Q_i at the segmented point of bolt is calculated using equation (7), which can be exerted on rock elements in an opposite direction to simulate the transverse support effect of bolts. The three components of Q_i in the global coordinate system are given as

$$\{Q_i^x \quad Q_i^y \quad Q_i^z\}^{\mathrm{T}} = \{p_i \quad s_i \quad w_i\}^{\mathrm{T}} Q_i, \tag{35}$$

where p_i, s_i, and w_i are the directional cosines of transverse deformation at segmented points of the bolt.

In accordance with interpolation theory of shape function, the support reaction force exerted on the rock by the i-th segmented point of the bolt is expressed as

$$f_{\mathrm{mg}} = -N_j T_i^k - N_j Q_i^k, \tag{36}$$

where N_j is the value of the shape function at the j-th node of the rock element at the segmented point of the bolt. T_i^k and Q_i^k are the components of T_i and Q_i in the directions of x, y, and z in the global coordinate system, respectively.

4.2. Calculation Procedure

(1) The seismic response results with bolt support in the $n-1$-th time step are obtained, and the free deformation of the surrounding rock without support in the n-th time step can be obtained by solving equation (31). On the basis of rock displacement, transverse displacement v_i and axial displacement u_r^i at the segmented points of the bolt are obtained using interpolation theory of finite element shape function. The Q_i and τ_i of bolts are, respectively, calculated by equations (7), (23), and (29), and the support force f_{mg} in the transverse and axial directions is deduced.

(2) The support force f_{mg} is exerted on the surrounding rock in the n-th time step. The model is resolved with equation (32), the displacement of the surrounding rock in the n-th time step with bolt supports is obtained, and this displacement is the real deformations of rock with bolts support during an earthquake.

The detailed calculation procedure is shown in Figure 5.

5. Verification of the Numerical Model of the Bolt

5.1. Example 1.
Zhao et al. [30] conducted a bolt pullout test and studied the distribution of axial force and shear stress along the axial direction of the bolt under different pullout forces. In the three test groups, the tensile force N_0 is 80, 160, and 240 kN, respectively; the physical and mechanical parameters of the materials are shown in Table 1.

During the test, the bolt was not subjected to transverse force, and l_i could be considered approximately equal to L of the bolt. Therefore, equation (19) can be rewritten as

$$\varepsilon_a(x) = \frac{N(x)}{EA_a}. \tag{37}$$

Equation (37) is combined with equation (20), and the differential equation is expressed as

$$\frac{\mathrm{d}^2 N(x)}{\mathrm{d}x^2} - \frac{\pi DK}{EA_a} N(x) + \pi DK \frac{\mathrm{d}u_r(x)}{\mathrm{d}x} = 0. \tag{38}$$

In the test, the bolt was buried in the fixed concrete, i.e., $u_r(x) = 0$. Therefore, equation (38) can be written in a matrix form as

$$[M'][N] + [G] = 0, \tag{39}$$

where

$$[M'] = \begin{bmatrix} -(2 + \alpha_e h^2) & 1 & & & & \\ 1 & -(2 + \alpha_e h^2) & 1 & & & \\ \ddots & & \ddots & & \ddots & \\ & & 1 & -(2 + \alpha_e h^2) & 1 & \\ & & & 1 & -(2 + \alpha_e h^2) \end{bmatrix},$$

$$\alpha_e = \frac{\pi DK_1}{EA_a}. \tag{40}$$

The anchoring interface is supposed to be in the elastic stage, and $K = K_1$. On the basis of the parameters of rock, mortar, and bolt, K_1 can be calculated using equations (10) and (11); $K_1 = 5$ GPa/m. The comparison of numerical values with the test values of the axial force and stress of the anchoring interface are shown in Figure 6. The numerical values of axial force and shear stress are nearly consistent with those of the test values, indicating that the bolt algorithm proposed in this study can accurately simulate bolt force in a pullout test.

5.2. Example 2.
A transverse shear test of bolts in jointed rock mass [31] is conducted to study the mechanical behavior of bolts. The schematic of the test model is shown in Figure 7 in which the transverse shear force Q_o is 102, 128, and 154 N, respectively. The distribution of the axial
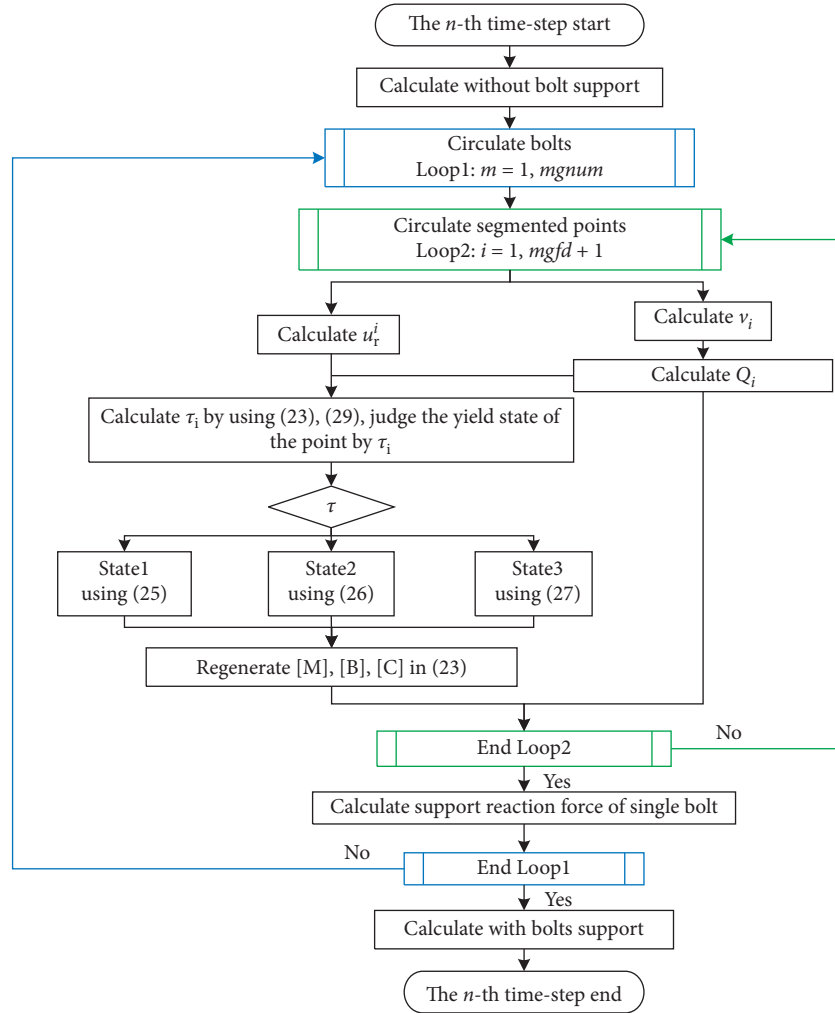
FIGURE 5: Flowchart of seismic response in surrounding rock with bolts support.

TABLE 1: Physical and mechanical parameters.

	Bolt		Mortar		Rock
L	3 m	t	55 mm	E_r	50 GPa
D_b	28 mm	E_m	18 GPa		
σ_{el}	400 MPa				
E_b	41 GPa				

strain of bolts is obtained by strain gauges 1–3, which are fixed on the bolt, and strain gauge 2 is close to the joint surface. The parameters of the materials are provided in Table 2.

The bolt is divided into four equal segments and five segmented points to calculate the axial strain of the bolt using the proposed algorithm. The positive direction is from strain gauge 1 to strain gauge 3, and the segmented point 3 is located on the joint surface. The value of plastic hinge section l_3 at segment point 3 is obtained. With the value of Q_o, the transverse displacement v_o at the joint surface can be calculated using (7). Supposing the anchoring interface is in the elastic stage, the transverse displacement in segmented point 3 is $v_3 = v_o$ and the transverse displacements at the other four segmented points are 0. The mortar is not considered in this test; therefore, the expression of K_1 can be rewritten as $K_1 = K_r/2$. On the basis of the material parameters, $K_1 = 2.5$ GPa/m is taken, and the other parameters are consistent with the test.

Axial force $N_1 - N_5$ at the segmented points can be obtained by solving (23), and axial force N_i and transverse shear force Q_i are substituted into (18) to obtain the axial displacements $u_a^1 - u_a^5$ at the segmented points. Axial strains $\varepsilon_a^1 - \varepsilon_a^5$ of the bolt at segmented points are obtained by geometric relations. The comparison of numerical values with the test values of the axial strain of the bolt is shown in Figure 8.

The distribution curves of the axial strain of the bolt, which are obtained from the test and calculation, show a trend of "large in the middle and small at both sides." The closer the bolt is to the joint, the greater its axial strain. The axial strains of the bolt at the segmented points are obtained by the numerical method in this study and consistent with the strains measured by the test, indicating that the proposed algorithm can accurately simulate bolt deformation in a shear test.

(a)

(b)
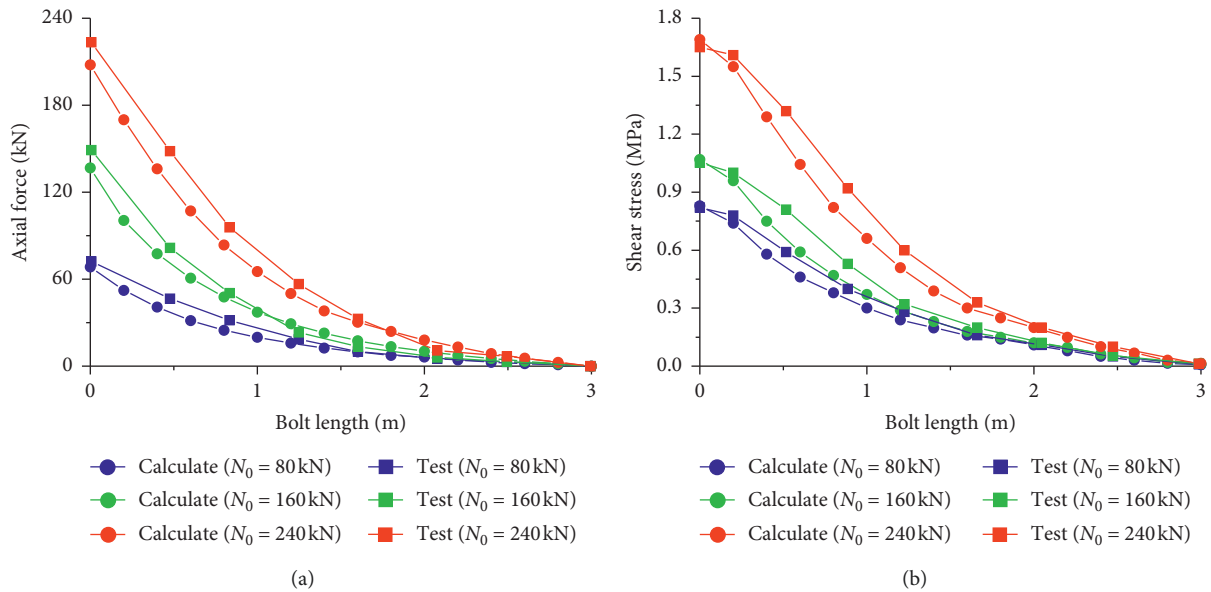
FIGURE 6: Distribution of the axial force and shear stress of the bolt.
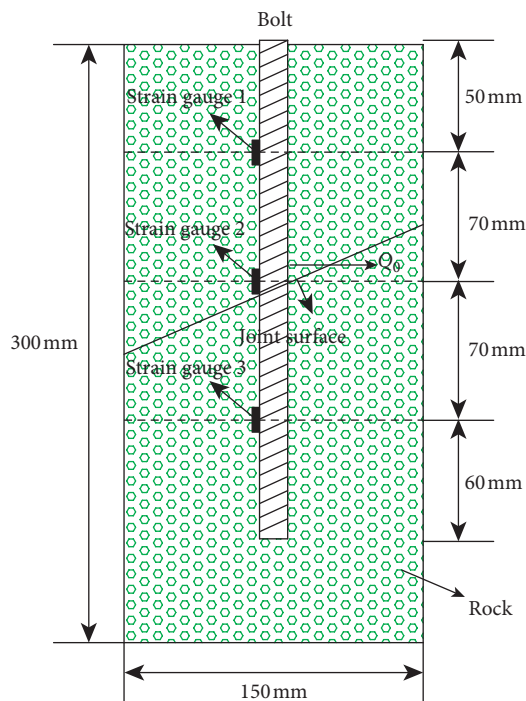
FIGURE 7: Schematic of the shear test of bolts. (a) Calculation model. (b) Excavation model.
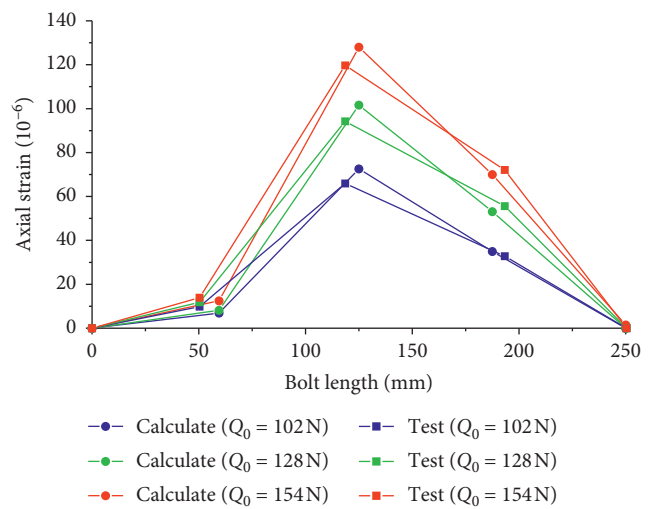

FIGURE 8: Distribution of the axial strain of the bolt.

6. Engineering Case Study

6.1. Engineering Profile. Figure 9 shows the FEM model of 3# of an underground powerhouse. The model is mainly composed of the main powerhouse, main transformer cavern, and surrounding rock. The sizes of the main powerhouse and main transformer cavern are $34.5\,\text{m} \times 30.0\,\text{m} \times 84.2\,\text{m}$ (length × width × height) and $34.5\,\text{m} \times 18.5\,\text{m} \times 34.2\,\text{m}$, respectively. The model consists of 25,839 nodes and 22,710 hexahedron elements (eight nodes). The maximum mesh size is $10\,\text{m}$ which meets the required dynamic calculation accuracy. The calculation ranges of the x, y, and z directions are 289.3, 47.6, and 294.1 m, respectively. The buried depth of the underground powerhouse is approximately $150\,\text{m}$. The region where the project

TABLE 2: Physical and mechanical parameters.

Bolt		Rock	
L	250 mm	σ_c	40 MPa
D_b	8 mm		
σ_{el}	400 MPa		
E_b	69 GPa		
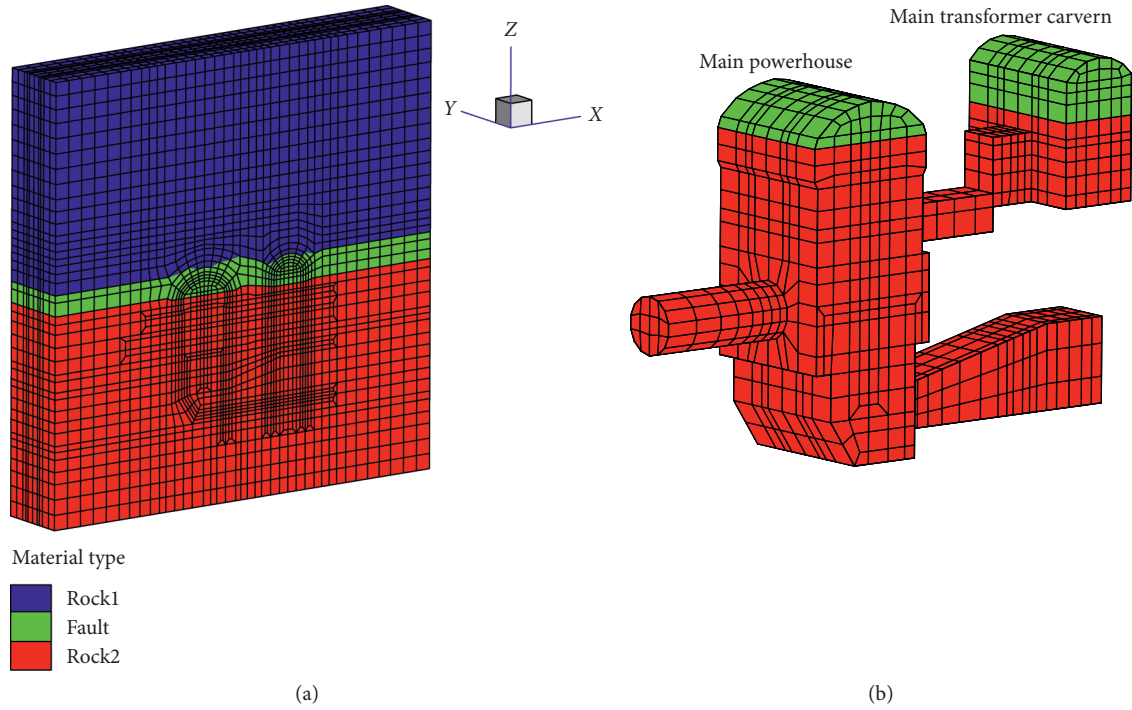
Figure 9: 3D FEM model of underground caverns. (a) Calculation model. (b) Excavation model.

is located is earthquake prone, with a basic seismic intensity of VII. The initial geostress field is obtained via stress inversion of the measured points. The disturbing stress field after the excavation of the underground caverns is considered the initial condition for dynamic calculation. The blue elements are rock 1, the red elements are rock 2, and the green elements at the top arch of the cavern are fault. The middle section of the model is selected as the typical section, in which six monitoring points on the surrounding rock of the main powerhouse and main transfer cavern are taken as research objects (shown in Figure 10) to study the stress and deformation of bolts and the stress and displacement response of the surrounding rock.

6.2. Calculation Conditions.

The elastic-plastic damage constitutive relation based on the Mohr–Coulomb criterion is adopted for surrounding rocks, and the scalar damage coefficient D is expressed as [29].

$$D = \sqrt{D_1^2 + D_2^2 + D_3^2},$$

$$D_i = 1 - \exp\left(-R\sqrt{\left(\varepsilon_i^p - \varepsilon_0^p\right)^2}\right), \quad i = 1, 2, 3,$$

$$\varepsilon_0^p = \frac{\left(\varepsilon_1^p + \varepsilon_2^p + \varepsilon_3^p\right)}{3},$$

(41)

where D_i is the damage coefficient of each principal stress direction, ε_i^p is the plastic bias strain in the i-th principal strain direction, and R is the material damage constant.

The bolts in the main caverns are arranged alternately in accordance with @1.5 m × 1.5 m, L = 6 m/9 m. The physical
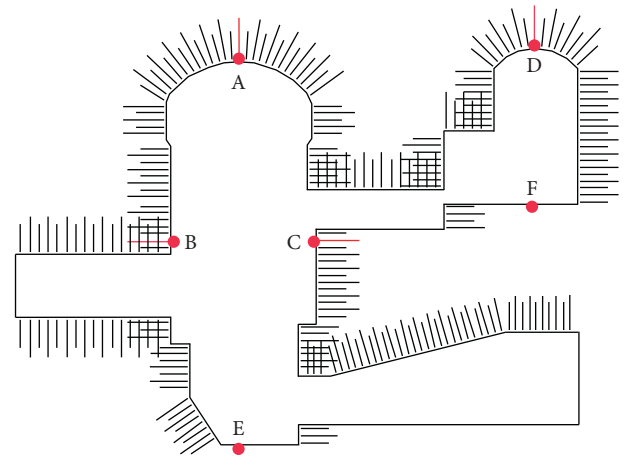
Figure 10: Layout of monitoring points.

and mechanical parameters of materials are shown in Table 3. A few bolts at the top arch of the caverns span two different rock mass materials, rock mass 1, and fault. The interfaces between all bolts and the surrounding rock are supposed to be K_1 = 3 GPa/m, K_2 = 2 GPa/m, τ_1 = 2.0 MPa, and τ_2 = 1.4 MPa to simplify the calculation. The input acceleration and displacement time history (shown in Figure 11) are synthesized in accordance with the seismic ground motion criterion of 5% exceedance probability in 50 years. The seismic wave is input from the bottom of the model. The x direction seismic waves are shown in Figure 11, and the z direction seismic waves are 2/3 that of the x direction. The viscoelastic artificial boundary is applied to the bottom of the model, the top is the free surface, and the

TABLE 3: Physical and mechanical parameters.

	Rock 1		Fault		Rock 2		Mortar		Bolt		Interface
E_r	15 GPa	E_r	5 GPa	E_r	17.5 GPa	E_m	10 GPa	E_b	210 GPa	c_i	0.8 MPa
μ_r	0.25	μ_r	0.3	μ_r	0.25	μ_m	0.167	σ_{el}	360 MPa	φ_i	30°
c_r	1.3 MPa	c_r	0.3 MPa	c_r	1.4 MPa	t	8 mm	D_b	28 mm		
φ_r	47.5°	φ_r	26.6°	φ_r	48.2°						
σ_t	2 MPa	σ_t	0.6 MPa	σ_t	2.4 MPa						
σ_c	60 MPa	σ_c	30 MPa	σ_c	70 MPa						
K_1	3 GPa/m			K_1	3 GPa/m						
K_2	2 GPa/m			K_2	2 GPa/m						

(a)

(b)
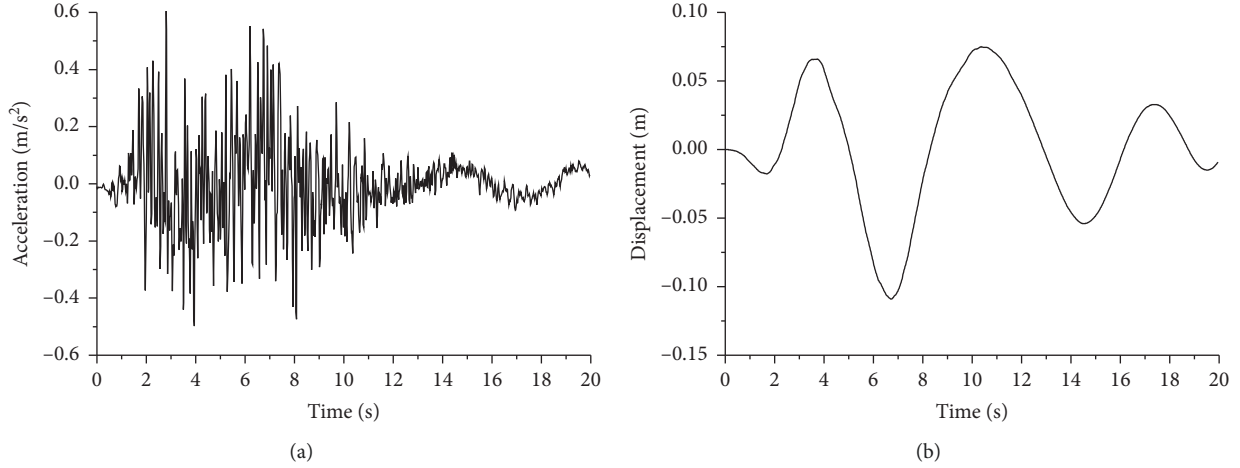
FIGURE 11: Time-history of the input acceleration and displacement.

free field artificial boundary is applied at the other sides. The bolt dynamic algorithm proposed in this study is embedded into a dynamic FEM numerical simulation platform [29] to study seismic calculation with support bolts.

6.3. Seismic Response of Underground Caverns under Different Support Conditions. The influence of bolts on the anti-seismic reinforcement of the surrounding rock is studied under three conditions: (1) without bolt, (2) considering only the axial deformation of bolt (the axial bolt algorithm), and (3) considering both the axial and transverse deformations of the bolt.

In condition (2), the transverse deformation of the bolt is not considered; thus, transverse force can be considered to be approximately 0, and l_i can be considered approximately equal to the length of the bolt. Therefore, control equation (20) can be transformed into equation (38), which can be rewritten in a matrix form as

$$[M''][N] + [B][\Delta u_r] + [G] = 0, \tag{42}$$

where

$$[M''] = \begin{bmatrix} -\chi & 1 & & & \\ 1 & -\chi & 1 & & \\ \ddots & \ddots & \ddots & & \\ & & 1 & -\chi & 1 \\ & & & 1 & -\chi \end{bmatrix}, \tag{43}$$

in stage 1, $\chi = 2 + (\pi DK_1/EA_a)h^2$; in stage 2, $\chi = 2 - (\pi DK_2/EA_a)h^2$. The other parameters are consistent with those in Section 3.

6.3.1. Analysis on the Axial Force of Bolts. The distribution regularities of the normal and shear stress of bolts A and B under conditions (2) and (3) conform to neutral point theory. The maximal normal stress appears at the neutral point, whereas the shear stress at both sides of the bolts reaches the maximum, as shown in Figure 12. Under condition (3), the maximal normal stress of bolt A increases considerably compared with that of condition (2), whereas the maximal normal stress of the bolt B increases slightly. Bolt A at fault has a large transverse deformation, whereas the transverse deformation of bolt B at the sidewall is small. The axial and transverse deformation of the bolt both contribute to the axial force for the algorithm in this study. Therefore, using the proposed algorithm can improve the support effect of bolts on the surrounding rock in the axial direction.

6.3.2. Analysis on the Transverse Force of Bolts. Using the bolt algorithm proposed in this study, Figure 13 shows the distribution regularity of the transverse deformation and force of bolts A, B, C, and D after an earthquake. Bolts A and D located at fault have large transverse deformation and force near the interface between the fault and rock 1, and bolts B and C at the sidewall have almost
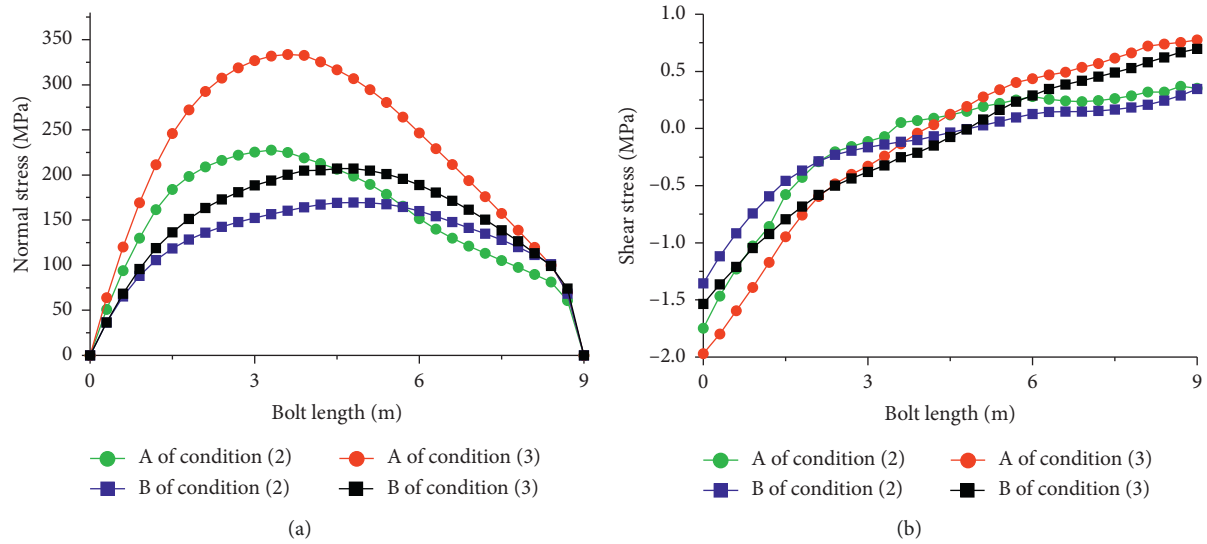
FIGURE 12: Stress distributions of monitoring bolts A and B. (a) Axial force stress. (b) Axial shear stress.

no transverse deformation and force. A transverse deformation of bolts can produce transverse force, which is the key to restraint dislocation between fault and rock mass. The bolts that pass through faults or joints undergo large transverse deformation at joints under seismic loads. Therefore, the axial bolt algorithm cannot fully reflect the support effect in a complex rock mass environment. The dynamic bolt algorithm, which considers both axial and transverse deformations, is necessary for practical engineering.

6.3.3. Displacement Response of Surrounding Rock. In this study, the relative displacement of monitoring points with the corresponding center points (E and F) of the floor on the typical section in the x direction is taken to reflect the deformation law of surrounding rock. Figure 14(a) shows the relative displacement time history of points A and B with the corresponding center point E under three different conditions. The three time-history curves of point A are different in amplitude, whereas the three curves of point B are similar in waveform and wave distribution. The relative displacement peak of monitoring points (A, B, C, and D) is shown in Figure 14(b). The relative displacement peak of points A and D under condition (3) is lower than that under conditions (1) and (2), whereas the relative displacement peak of points B and C at the sidewall has minimal difference under the three conditions. The bolt algorithm has an inconsiderable influence on the numerical results of sidewall deformation, but considering the transverse deformation and force of bolts can effectively reduce the deformation of fault at the top arch.

6.3.4. Stress Response of Surrounding Rock. The tensile strength of rock is much smaller than its compressive

strength; thus, tension fracture is a common failure form of rock material. The maximum principal stress time histories of point A under three conditions are taken for analysis (as shown in Figure 15(a)). The maximum principal stresses are mainly compressive stresses, and the fluctuation amplitudes of these curves are small in the period of 0–1.8 s. From 1.8 s to 7.2 s, the curves fluctuate violently, with their fluctuation ranging from −0.46 MPa to 0.82 MPa. In the period of 7.2–20 s, the fluctuation tends to be steady. A comparison of Figures 11(a) and 15(a) shows that the time when the maximum principal stress at point A occurs under the three conditions is consistent with the time when maximum acceleration occurs. The maximum principal stress time-history curves are similar to the input acceleration curve, indicating that the stress response of the surrounding rock is affected by the input seismic wave. The stress responses are greatly different for point A under three conditions. The fluctuations of maximum principal stress are most intense under condition (1), and the fluctuations are lowest under condition (3). The effects of bolt support on the peak values of maximum principal stresses are shown in Figure 15(b). The peak values of the maximum principal stress decrease considerably when considering bolt support. The peaks of the maximum principal stress of the top arches (points A and D) under condition (2) are larger than those under condition (3), whereas the peaks of the maximum principal stress of the sidewalls (points B and C) are not much different under conditions (2) and (3). Hence, the stress response of fault can be reduced effectively by using the bolt algorithm proposed in this study.

6.3.5. Damage Coefficient of Surrounding Rock. The damage coefficient of surrounding rock can directly reflect its
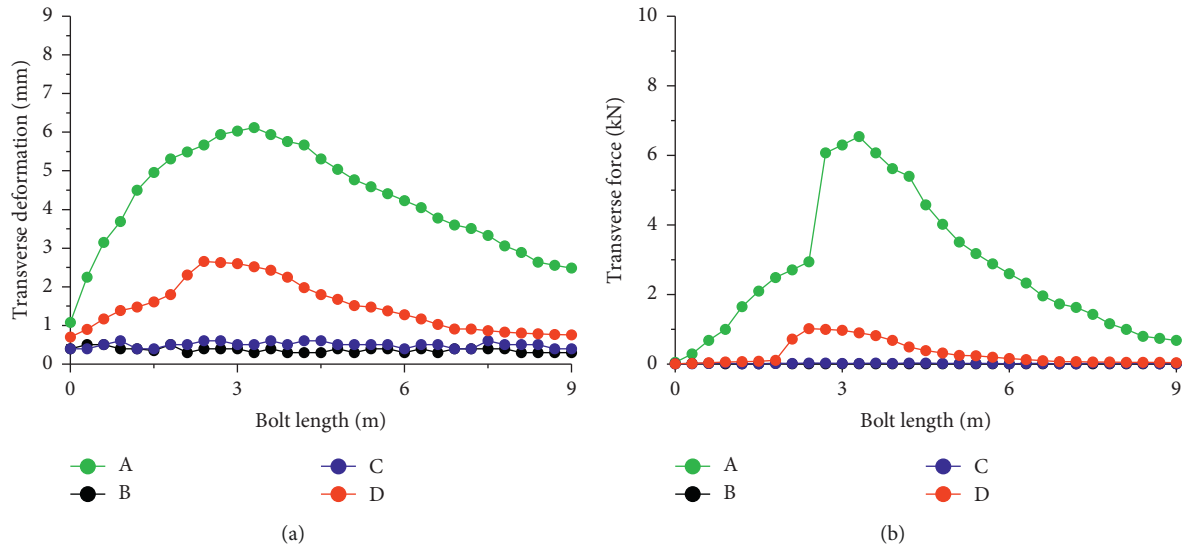
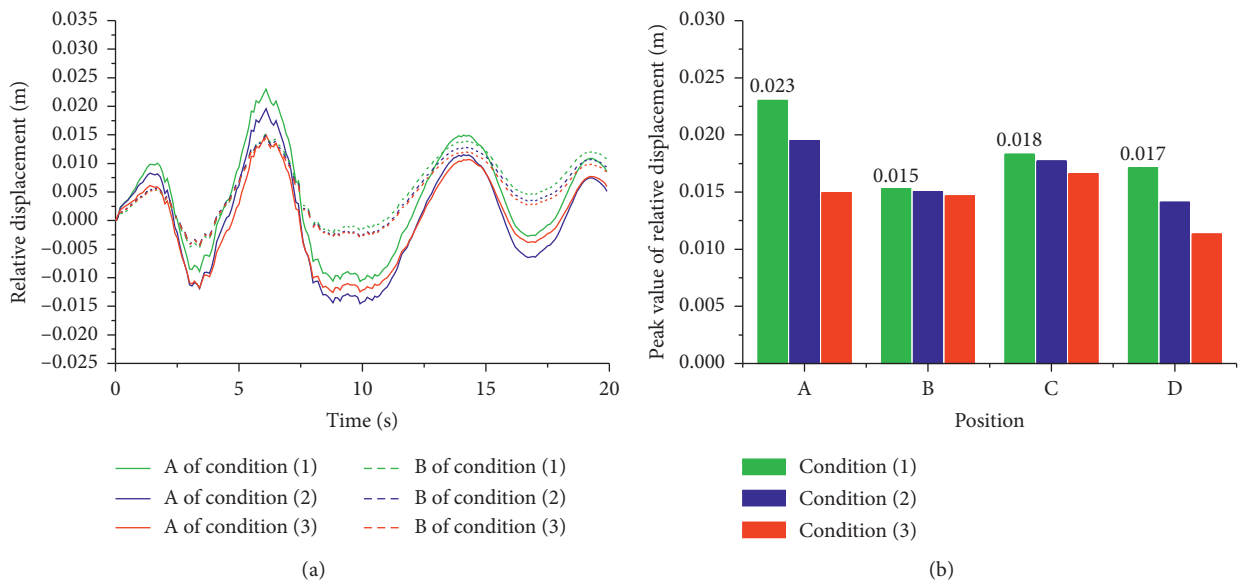FIGURE 13: Transverse deformation and force of monitoring bolts.

FIGURE 14: Displacement response under different conditions. (a) Relative displacement time histories of monitoring points A and B in the x direction. (b) Peak values of relative displacement for monitoring points in the x direction.

seismic damage degree. The distributions of damage coefficient on the typical section under three conditions after the earthquake are plotted in Figure 16. The damage zone without bolt support is mainly distributed at the top arches and sidewalls of the main powerhouse and main transformer cavern and the intersection of the main powerhouse with tailrace tunnel, diversion tunnel, and main electrical wire hall (as shown in Figure 16(a)). The damage coefficient for majority of the area is approximately 0.5. Damage is most serious at the top of the caverns, which are crossed by fault, and the maximum damage coefficient exceeds 0.9. When considering the axial support of bolts, the damage area and degree of surrounding rock are

considerably reduced, while the damage coefficient of sidewalls and the intersections of caverns are reduced to 0.3. However, the damage coefficient of the top arches remains large; the maximum of which is approximately 0.8 (as shown in Figure 16(b)). Compared with Figure 16(b), Figure 16(c) depicts that the damage degree, which is obtained by the proposed bolt algorithm, at the top arches of the caverns is considerably reduced. The damage coefficient for majority of the top arches is approximately 0.3, and the maximum damage coefficient does not exceed 0.5. Therefore, the transverse support of bolts can effectively reduce the damage degree of the surrounding rock at the fault under seismic load.
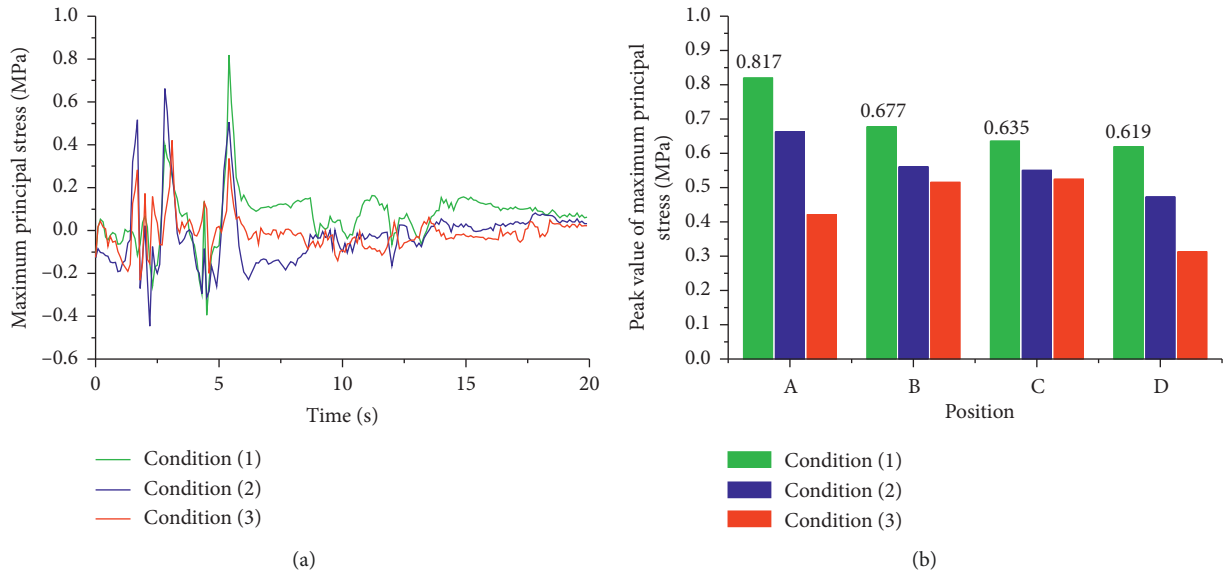
(a)

(b)

FIGURE 15: Maximum principal stress under different conditions. (a) Stress time histories of point A. (b) Peak values of maximum principal stress.
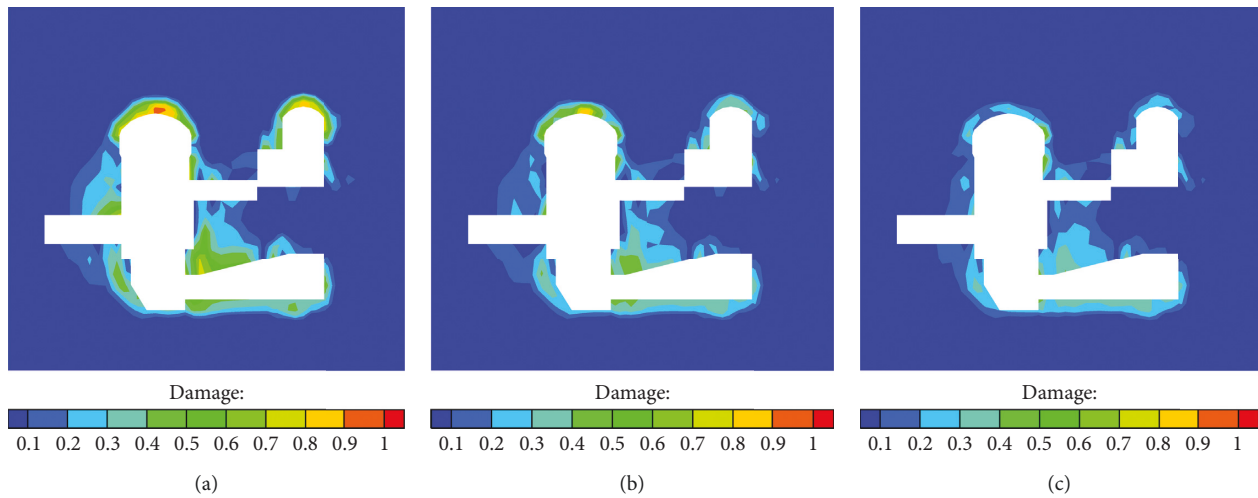

(a)

(b)

(c)

FIGURE 16: Damage coefficient distribution of typical section under different conditions.

7. Conclusions

On the basis of classical beam theory and the trilinear shear slip model, a new dynamic algorithm that considers the axial and transverse deformations of bolts is proposed. The algorithm is applied to the seismic support analysis of an underground project, and the following conclusions are drawn:

(1) The proposed dynamic algorithm fully considers the characteristic of slippage and yield of interface between the anchorage body and surrounding rock and the transverse deformation characteristic of bolts. The algorithm can effectively simulate the stress and deformation of bolts located at faults or joints under seismic load. The rationality and feasibility of the

dynamic algorithm are verified through comparison using pullout data and a shear test of bolts.

(2) The distribution of the axial normal and shear stresses of bolts obtained by the proposed algorithm is similar to the results calculated by the axial bolt algorithm; both of which fit in with neutral point theory. However, the proposed algorithm is more effective in restraining the surrounding rock in the axial direction of the bolts due to the contribution of the transverse deformation to the axial force. The bolts located at the fault have large transverse deformation, whereas the bolts located at the rock without joint or fault have no transverse deformation. This result indicates that the transverse deformation of bolts in complex rock environment

conditions during an earthquake should be considered.

(3) Bolt support can effectively reduce the x directional deformation of the fault at the top arches of the caverns, and exerts a minimal effect on the sidewalls. The x directional deformation of the top arches under earthquake calculated by the proposed bolt algorithm is lower than that calculated by the axial bolt algorithm, which indicates that the transverse force of bolts affects the restriction of the mutual slip of rock masses at the fault. After considering bolt support, the maximum principal stress of the surrounding rock is considerably reduced under seismic load, and the reduction extent of the maximum principal stress of the fault calculated by the proposed bolt algorithm is greater than that calculated by the axial bolt algorithm. Considering bolt support can effectively reduce the damage degree of the entire underground caverns, and the reduction extent of damage for the surrounding rock at the fault calculated by the proposed bolt algorithm is more remarkable than that calculated by the axial bolt algorithm.

Data Availability

The data used to support the findings of this study are available from the corresponding author upon request.

Conflicts of Interest

The authors declare that there are no conflicts of interest regarding the publication of this paper.

Acknowledgments

References

[1] G. Q. Liu, M. Xiao, J. T. Chen, and H. Zhou, "Study on mechanical characteristics of fully grouted rock bolts for underground caverns under seismic loads," *Mathematical Problems in Engineering*, vol. 2017, Article ID 1657369, 12 pages, 2017.

[2] H. Zhou, M. Xiao, and J. T. Chen, "Study of the anchoring mechanism and the analysis of the anchoring effect of the fully grouted rock anchor in large-scale underground caverns," *Rock and Soil Mechanics*, vol. 37, no. 5, pp. 1–9, 2016.

[3] T. J. Freeman, "The behavior of fully-bonded rock bolts in the fielder experimental tunnel," *Tunnels and Tunneling*, vol. 10, no. 5, pp. 37–40, 1978.

[4] G. Rong, H. C. Zhu, and C. B. Zhou, "Testing study on working mechanism of fully grouted bolts of thread steel and smooth steel," *Chinese Journal of Rock Mechanics and Engineering*, vol. 23, no. 3, pp. 459–475, 2004.

[5] A. Kilic, E. Yasar, and A. G. Celik, "Effect of grout properties on the pull-out load capacity of fully grouted rock bolt," *Tunnelling and Underground Space Technology*, vol. 17, no. 4, pp. 355–362, 2002.

[6] L. B. Martin, M. Tijani, and F. Hadj-Hassen, "A new analytical solution to the mechanical behaviour of fully grouted rock bolts subjected to pull-out tests," *Construction and Building Materials*, vol. 25, no. 2, pp. 749–755, 2011.

[7] J. Chen, S. Saydam, and P. C. Hagan, "An analytical model of the load transfer behavior of fully grouted cable bolts," *Construction and Building Materials*, vol. 101, pp. 1006–1015, 2015.

[8] J. Nemcik, S. Ma, N. Aziz, T. Ren, and X. Geng, "Numerical modelling of failure propagation in fully grouted rock bolts subjected to tensile load," *International Journal of Rock Mechanics and Mining Sciences*, vol. 71, pp. 293–300, 2014.

[9] F. F. Ren, Z. J. Yang, J. F. Chen, and W. W. Chen, "An analytical analysis of the full-range behaviour of grouted rockbolts based on a tri-linear bond-slip model," *Construction and Building Materials*, vol. 24, no. 3, pp. 361–370, 2010.

[10] W. Q. Chen, Y. F. Zhao, and J. J. Zhao, "Shear resistance theory of bolt considering nonlinear behaviour of grout reaction force," *Rock and Soil Mechanics*, vol. 39, no. 5, pp. 1662–1668, 2018.

[11] H. Jalalifar, N. Aziz, and M. Hadi, "The effect of surface profile, rock strength and pretension load on bending behaviour of fully grouted bolts," *Geotechnical and Geological Engineering*, vol. 24, no. 5, pp. 1203–1227, 2006.

[12] A. M. Ferrero, "The shear strength of reinforced rock joints," *International Journal of Rock Mechanics and Mining Sciences and Geomechanics Abstracts*, vol. 32, no. 6, pp. 595–605, 1995.

[13] X. Li, N. Aziz, A. Mirzaghorbanali, and J. Nemcik, "Behavior of fiber glass bolts, rock bolts and cable bolts in shear," *Rock Mechanics and Rock Engineering*, vol. 49, no. 7, pp. 2723–2735, 2016.

[14] Q. S. Liu, G. F. Lei, X. X. Peng, L. Wei, J. P. Liu, and Y. C. Pan, "Experimental study and mechanism analysis of influence of bolt anchoring on shear properties of jointed rock mass," *Rock and Soil Mechanics*, vol. 38, no. 2, pp. 33–41, 2017.

[15] Y. Chen, "Experimental study and stress analysis of rock bolt anchorage performance," *Journal of Rock Mechanics and Geotechnical Engineering*, vol. 6, no. 5, pp. 428–437, 2014.

[16] W. Zhang and Q. S. Liu, "Analysis of deformation characteristics of prestressed anchor bolt based on shear test," *Rock and Soil Mechanics*, vol. 35, no. 8, pp. 2231–2240, 2014.

[17] F. Pellet and P. Egger, "Analytical model for the mechanical behaviour of bolted rock joints subjected to shearing," *Rock Mechanics and Rock Engineering*, vol. 29, no. 2, pp. 73–97, 1996.

[18] H. Jalalifar and N. Aziz, "Analytical behaviour of bolt-joint intersection under lateral loading conditions," *Rock Mechanics and Rock Engineering*, vol. 43, no. 1, pp. 89–94, 2010.

[19] X. R. Ge and J. B. Liu, "Study on the shear resistance behaviour of bolted rock joints," *Chinese Journal of Geotechnical Engineering*, vol. 10, no. 1, pp. 8–19, 1988.

[20] W. Zhang and Q. S. Liu, "Synthetical deformation analysis of anchor bolt in jointed rock mass," *Rock and Soil Mechanics*, vol. 33, no. 4, pp. 1067–1074, 2012.

[21] G. Q. Liu, M. Xiao, J. T. Chen, and H. Zhou, "Stress analysis method of fully grouted rock bolt in underground caverns," *Journal of Huazhong University of Science and Technology (Natural Science Edition)*, vol. 45, no. 6, pp. 113–116, 2017.

[22] G. Q. Liu, M. Xiao, and H. Zhou, "Simulation of fully grouted rock bolts using dynamic finite element for underground

caverns," *Chinese Journal of Rock Mechanics and Engineering*, vol. 36, no. 1, pp. 61–70, 2017.

[23] H. Zhou, M. Xiao, and J. Chen, "Analysis of a numerical simulation method of fully grouted and anti-seismic support bolts in underground geotechnical engineering," *Computers and Geotechnics*, vol. 76, pp. 61–74, 2016.

[24] M. Xiao, "3-D elastoplastic FEM analysis of implicit cylindric anchor bar element for underground opening," *Chinese Journal of Geotechnical Engineering*, vol. 14, no. 5, pp. 19–26, 1992.

[25] B. Y. Yang, M. Xiao, N. Luo, and X. W. Wang, "Research on mechanical characteristic of anchor bolt in process of shearing," *Journal of Huazhong University of Science and Technology (Natural Science Edition)*, vol. 47, no. 3, pp. 127–132, 2019.

[26] S. Ma, Z. Zhao, W. Nie, and Y. Gui, "A numerical model of fully grouted bolts considering the tri-linear shear bond-slip model," *Tunnelling and Underground Space Technology*, vol. 54, pp. 73–80, 2016.

[27] Q. Yang, X. G. Zhu, and M. T. Luan, "Development of hyperbolic model for fully grouting rock bolt and parameters analysis for anchoring effect," *Chinese Journal of Rock Mechanics and Engineering*, vol. 26, no. 4, pp. 692–698, 2007.

[28] X. L. Ding, Q. Sheng, J. Han, L. K. Chen, and S. W. Bai, "Numerical simulation testing study on reinforcement mechanism of prestressed anchorage cable," *Chinese Journal of Rock Mechanics and Engineering*, vol. 21, no. 7, pp. 980–988, 2002.

[29] Z. G. Zhang, M. Xiao, and J. T. Chen, "Simulation of earthquake disaster process of large-scale underground caverns using three-dimensional dynamic finite element method," *Chinese Journal of Rock Mechanics and Engineering*, vol. 30, no. 3, pp. 509–523, 2011.

[30] T. Y. Zhao, X. Y. Bai, M. Y. Zhang, X. Y. Chen, and K. K. Jia, "Field test and numerical simulation of bearing capacity of steel reinforcement anti-floating anchor," *Science Technology and Engineering*, vol. 18, no. 7, pp. 38–43, 2018.

[31] L. H. Chen, *Study on the load transfer behavior of the rock bolt and its anchoring efficacy in jointed rock mass around highway tunnel*, Ph.D. thesis, Chongqing University, Chongqing, China, 2016.